Research Article Vol. 59, No. 7 / 1 March 2020 / Applied Optics 1985

applied optics

Anti-stain algorithm of angular displacement based on a single image sensor

Hai Yu,* Qiuhua Wan, Changhai Zhao, Xinran Lu, and Ying Sun

Changchun Institute of Optics, Fine Mechanics and Physics, Chinese Academy of Sciences, Changchun 130033, China
**Corresponding author: yuhai@ciomp.ac.cn*

Received 20 November 2019; revised 25 January 2020; accepted 26 January 2020; posted 27 January 2020 (Doc. ID 383765); published 25 February 2020

The displacement measuring technique is prone to failure within the industrial environment due to the influence of dust, oil, and other contaminants that stain the equipment. There is urgent demand for new anti-stain techniques. In today's image angular displacement measurement technology, the pixel array is used instead of the traditional photoelectric conversion element; this creates room for anti-stain improvement based on the image processing components. Based on a previous study on image-type angular displacement measurement technology, a single head image-type anti-stain algorithm is proposed in this paper that can remove the interference of small stains and ensure correct measurement value outputs. The influence of the stain on the calibration grating is first assessed based on the principle of image angular displacement measurement technology. An anti-stain algorithm based on the metal grating and multi-line fusion is proposed accordingly. The proposed algorithm is then tested on a circular grating with 38 mm diameter and $2^N = 256$ lines in the circle. The results show that angle measurement output accuracy can be guaranteed when the number of lines covered by the stains is less than half of the coding-bits. This work may provide a technical basis for enhancing stain resistance in high-performance displacement measurement technology.

https://doi.org/10.1364/AO.383765

1. INTRODUCTION

Digital displacement measurement technology is an important element of industrial manufacturing, aerospace, military equipment, and other applications per its high precision, high resolution, wide measurement range, and compatibility with various other digital equipment [1,2]. Advancements in precision manufacturing technology have made the industrial environment increasingly complex; within this environment, displacement measuring equipment is prone to failure due to the influence of dust, oil, and other contaminants that stain the components. There is urgent demand for techniques to enhance stain resistance. Engineers in the basic manufacturing field seek innovative angular displacement measurement technology to improve the stain resistance of various industrial components.

Image-type angular measurement technology can achieve higher resolution than traditional measurement because it utilizes multi-pixel information. It can also be used to improve stain resistance. Leviton, for example, used area array CCD in a 2003 study to receive grating patterns with reference lines and binary symbols; the angular resolution of this setup is as high as 0.01″ [3,4]. Sugiyam *et al.* realized angle measurement resolution of 0.022° on a circular grating with 30 mm diameter based on a code location recognition technique in a 2008 study on the area array detector [5]. Jin *et al.* proposed superimposing a CMOS image array to form virtual moiré fringes, achieving a resolution of 0.1 μm and accuracy over 0.4 μm [6]. Baji *et al.* established a displacement measurement method based on color recognition to measure the rotation angle of a color-coated code disk, realizing angle measurement resolution of 0.1° [7]. In a more recent study, Kim *et al.* used the phase-shifting coding method and a micro image detection system to achieve 10-bit and 13-bit coding recognition [8].

The scholars discussed above used image recognition methods to realize displacement measurement. To date, there has been little research on stain resistance as it applies to these technologies. It is common practice to increase the sealing performance for the purposes of stain resistance, but it is difficult to achieve a complete seal due to the influence of the rotating bearing. The resolute series absolute grating ruler (RENISHAW Co.) has a steel band ruler and built-in redundancy code technology that can correctly read data in cases of light dust pollution; the ERA series absolute displacement measuring equipment (HEIDENHAN Co.) uses an optical scanning module to generate scanning signals in cases of local light pollution on the reference grating, which ensures that the output signal has no offset or phase change. In 2019, Yuan *et al.* proposed a subdivision algorithm with robust performance, which can remove small pollution, and its precision is 1.9″ [9].

In addition, magnetic grid technology can also improve the stain resistance [10], but is subject to electromagnetic interference and does not readily achieve high-precision measurement.

In a previous study, we proposed a subdivision algorithm based on quadratic function fitting [11]. We also proposed an angle displacement measurement method based on double image recognition that realized measurement resolution of 0.15″ and precision of 6.33″ on a 38 mm diameter code disk [12]. We have also explored displacement measurement using a super-resolution imaging method in our laboratory [13]. Our results altogether suggest that angular displacement measurement technology based on image sensors has higher measurement resolution and accuracy than the traditional measurement methods, but the extant research centers on angle measurement while neglecting anti-stain performance.

In this study, based on the extant research on image-type angular displacement measurement technology, we developed an anti-stain algorithm based on multi-line fusion. Experimental results show that the algorithm can effectively eliminate interference from grating stains. When the number of lines covered by the stains is less than half of the coding-bits, the interference of the stains can be effectively completely removed.

This paper is organized as follows: Section 2 discusses the effects of stains on image measurement efficacy, Section 3 presents the proposed algorithm, Section 4 reports our experimental results, and Section 5 provides a brief summary and conclusion.

2. STAIN INTERFERENCE MECHANISMS

A. Image Angular Displacement Measurement Principle

Typical image angular displacement measurement technology is shown in Fig. 1. The setup mainly includes a principal axis, calibration grating, parallel light, and linear image sensor. 2^N translucent lines with equal interval and radius are engraved on the calibration grating. The parallel light emitted by the parallel light source passes through the translucent lines on the calibration grating, and then projects a pattern onto the linear image sensor [12–14]. To ensure imaging quality, the distance between the linear image sensor and the calibration grating is kept below 0.5 mm.

Here, we propose a metal calibration grating coding method. It is necessary to realize absolute position coding on the calibration grating. We transformed the gridlines into "wide" and "narrow" gridlines to form "wide" coding lines and "narrow" coding lines, which represent coding of "1" and "0", respectively. The lines in the circle are arranged according to the pseudo-random shift code.

Set the value representing the i code as X_i; the adjacent eight X_i are coded in a group, just like $\{X_i, X_{i+1}, X_{i+2}, X_{i+3}, X_{i+4}, X_{i+5}, X_{i+6}, X_{i+7}\}$. When the grating moves, the coded group changes from $\{X_i, X_{i+1}, X_{i+2}, X_{i+3}, X_{i+4}, X_{i+5}, X_{i+6}, X_{i+7}\}$ to $\{X_{i+1}, X_{i+2}, X_{i+3}, X_{i+4}, X_{i+5}, X_{i+6}, X_{i+7}, X_{i+8}\}$. Within the circumference, we can get 2^8 coded groups. To make each set of codes unique, the value of each X_i is calculated by "XOR" operation of the first eight code values:

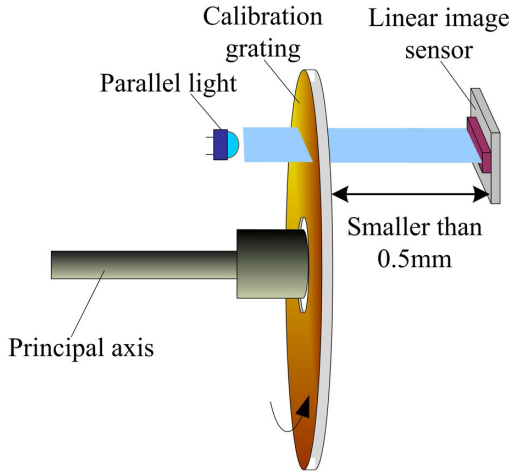

Fig. 1. Image-type measurement.

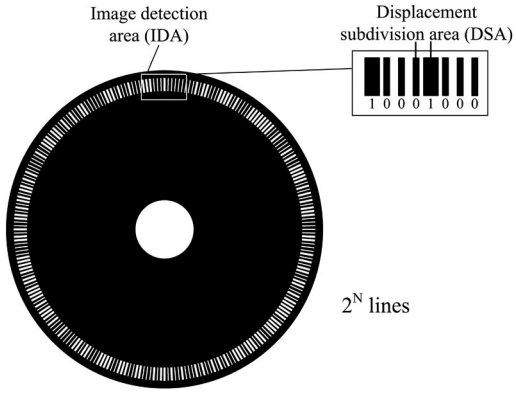

Fig. 2. Coding principle.

$$X_i = m_1 X_{i-1} \oplus m_2 X_{i-2} \oplus \cdots \oplus m_8 X_{i-8}, \quad (1)$$

where "⊕" represents the XOR operation and $m_1 - m_8$ are coefficients of operation (value "0" or "1"). If the coefficients $m_1 - m_8$ are selected reasonably, the decoding values of each group of codes with 2^8 different codes can be obtained.

By using MATLAB software, one of the expressions we used to calculate the code values is shown in Eq. (2):

$$X_i = X_1 \oplus X_2 \oplus X_3 \oplus X_8. \quad (2)$$

By Eq. (2), there are 2^8 coding lines in total, as shown in Fig. 2.

For each coded group, we set the decoding values as A; the A value is equal to i, so

$$A = i. \quad (3)$$

The linear image sensor contains at least eight lines in the image detection area (IDA) on the grating. The range between the lines on both sides of the image center point is the displacement division area (DSA), as shown in Fig. 3.

In Fig. 3, L_1 and L_2 are two adjacent lines in the DSA, x_0 is the center position of the image detector, and x_a and x_b are the centroids of two coding lines on both sides of the DSA, respectively. By subdividing the DSA, we can achieve higher resolution than the number of coded bits. The subdivision algorithm is

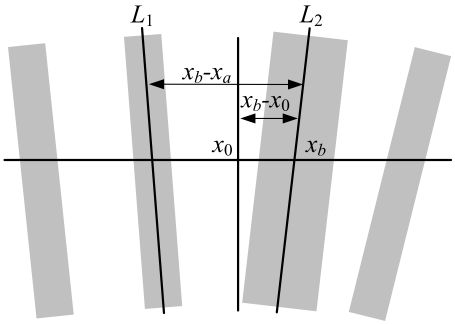

Fig. 3. DSA principle.

$$B = \frac{x_b - x_0}{x_b - x_a} \cdot 2^m, \tag{4}$$

where 2^m is the subdivision mapping value. The subdivision resolution is higher when a greater m value can be resolved. The angular displacement measurement is maximized by connecting values A and B. Finally, the output angular value is expressed as $D = A \cdot 2^m + B$.

B. Stain Interference

When the stain attached to the calibration grating appears in the IDA, the collected image is as shown in Fig. 4.

The lines on the calibration grating are transparent. The measurements are thus affected when stains block the calibration grating. The presence of stains affecting this system can be divided into the following three cases.

(1) When a large number of reference lines is covered by stains in the IDA (including those in the DSA), it is not possible to obtain decoding or subdivision values [Fig. 4(a)].
(2) When the stain only covers part of the lines but there is no stain in the DSA, it can be subdivided but not decoded [Fig. 4(b)].
(3) When the stain is small and only attached to the edge of the line, the encoded value can still be recognized; however, when the line in the DSA is blocked, the values of x_a and x_b change and the subdivision operation is greatly affected [Figs. 4(c) and 4(d)].

In essence, when there are stains in the IDA that block the lines, the image angular displacement measurement is incorrect.

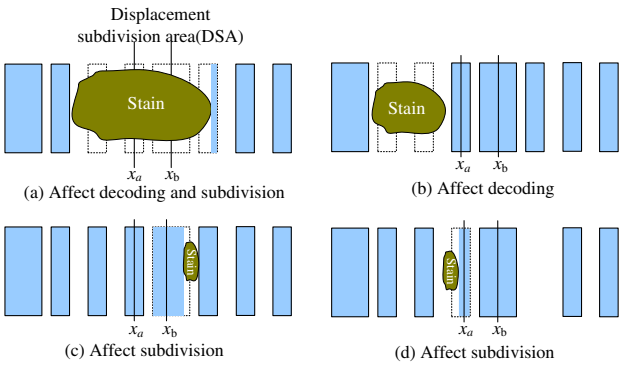

Fig. 4. Principle of stain interference.

3. STAIN RESISTANCE ALGORITHM

Although the "leakage" lines of the metal grating can resist dust, when there are particle stains attached to the grating, the light passing through is blocked, resulting in output errors. The proposed anti-stain algorithm was designed accordingly.

A. Stain Identification and Location

The premise of the anti-stain algorithm is to recognize and locate any stain on the calibration grating by image processing. Per the calibration grating shown in Fig. 2, the included angle between all adjacent lines is the same. When the number of lines in the circular grating is $2^n \geq 2^8$, the spacing of the lines collected by the linear array image sensor can be considered equal. When stains in the IDA block the lines, the collected image is as shown in Fig. 5.

In Fig. 5, the stain obscures three coding lines. By default, the spacing between adjacent lines is Δx and the width of "wide" lines is ΔL. After the linear array image sensor collects the image, it searches all the light transmission regions from left to right and calculates the respective centroids of the regions, which are recorded as $x_1, x_2, x_3, x_4, x_5, x_6, x_7$. The difference between adjacent centroids is then calculated as $\Delta_1 = x_2 - x_1$, $\Delta_2 = x_3 - x_2$, $\Delta_3 = x_4 - x_3$, $\Delta_4 = x_5 - x_4$, $\Delta_5 = x_6 - x_5$, $\Delta_6 = x_7 - x_6$. Here, we use $\Delta_1 - \Delta_6$ to identify the stains.

1. Stain Identification

Under normal circumstances, all $\Delta_1 - \Delta_6$ should be equal to Δx (or there is a small deviation); when there is a stain, the spacing of the lines changes. As shown in Fig. 4, there are $\Delta_1 < \Delta x$, $\Delta_2 > \Delta x$, $\Delta_3 < \Delta x$, $\Delta_4 - \Delta_6 = \Delta x$. A stain is identified when any value of $\Delta_1 - \Delta_6$ markedly changes.

2. Stain Positioning

It is necessary to use unpolluted lines in the IDA for location calculation to accurately place the stains. Consider Fig. 4 as an example. According to the $\Delta_1 - \Delta_6$ values, and as the values of Δ_4, Δ_5, and Δ_6 are normal, the lines represented by x_4, x_5, x_6, and x_7 are not polluted. Based on line x_4, all the lines that can be identified are scanned to realize the positioning. Set the location array to P[j], ($j = 1, 2, \ldots, 8$), so we have the following:

The value x_3 in the area of $\{x_4 - \Delta x + \Delta L/2,\ x_4 - \Delta x - \Delta L/2\}$, then P[4] = x_3, P[5] = x_4;

No value in the area of $\{x_4 - 2\Delta x + \Delta L/2,\ x_4 - 2\Delta x - \Delta L/2\}$, P[3] = 0, P[4] = x_3, P[5] = x_4;

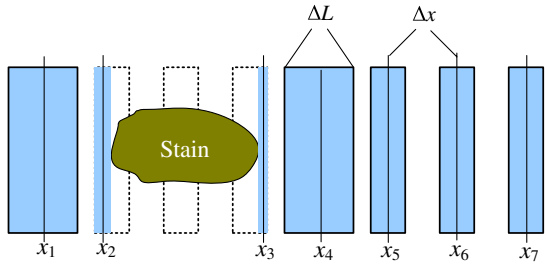

Fig. 5. Stain recognition.

The value x_2 is in the area of $\{x_4 - 3\Delta x + \Delta L/2,\ x_4 - 3\Delta x - \Delta L/2\}$, then $P[2] = x_2$, $P[3] = 0$, $P[4] = x_3$, $P[5] = x_4$;

The value x_1 is in the area of $\{x_4 - 4\Delta x + \Delta L/2,\ x_4 - 4\Delta x - \Delta L/2\}$, then $P[1] = x_1$, $P[2] = x_2$, $P[3] = 0$, $P[4] = x_3$, $P[5] = x_4$.

For the other side:

The value x_5 is in the area of $\{x_4 + \Delta x + \Delta L/2,\ x_4 + \Delta x - \Delta L/2\}$, then $P[1] = x_1$, $P[2] = x_2$, $P[3] = 0$, $P[4] = x_3$, $P[5] = x_4$, $P[6] = x_5$;

The value x_6 is in the area of $\{x_4 + 2\Delta x + \Delta L/2,\ x_4 + 2\Delta x - \Delta L/2\}$, then $P[1] = x_1$, $P[2] = x_2$, $P[3] = 0$, $P[4] = x_3$, $P[5] = x_4$, $P[6] = x_5$, $P[7] = x_6$;

The value x_7 is in the area of $\{x_4 + 3\Delta x + \Delta L/2,\ x_4 + 3\Delta x - \Delta L/2\}$, then $P[1] = x_1$ $P[2] = x_2$, $P[3] = 0$, $P[4] = x_3$, $P[5] = x_4$, $P[6] = x_5$, $P[7] = x_6$, $P[8] = x_7$.

Then, because $\Delta_1 < \Delta x$, $\Delta_2 > \Delta x$, $\Delta_3 < \Delta x$, let x_2 and x_3 be zero. Finally, the positioning array is $\{P[1], P[2], P[3], P[4], P[5], P[6], P[7], P[8]\} = \{x_1, 0, 0, 0, x_4, x_5, x_6, x_7\}$. In the array, the value "0" indicates that the line at this position is occluded.

B. Stain Resistance Algorithm

The anti-stain algorithm can be operated according to the calculated array P[1]−P[8]. When obtaining the measurement value, the coding value and subdivision value are first determined separately.

1. Calculation of Subdivision Value

In the subdivision operation, the key is to accurately determine the two centroids x_a and x_b in the DSA region. We propose a subdivision method based on multi-line fusion for this purpose. The principle is shown in Fig. 6.

Normally, the position of x_a coincides with P[4] on the left side of the image center position, while the position of x_b coincides with P[5] on the right side of the image center position, as shown in Fig. 6(a). When using the multi-line fusion algorithm, the array elements symmetrical to the position of x_a can be divided into four groups: {P[1], P[7]}, {P[2], P[6]}, {P[3], P[5]}, {P[4]}; the array elements symmetrical to the position of x_b can be divided into four groups: {P[2], P[8]}, {P[3], P[7]}, {P[4], P[6]}, {P[5]}. Then, x_a and x_b are calculated as follows:

$$x_a = \frac{\sum_{j=1}^{7} P[j]}{7}, \tag{5}$$

$$x_b = \frac{\sum_{j=2}^{8} P[j]}{7}. \tag{6}$$

The subdivision value is then calculated as $B = 2^m \cdot (x_b - x_0)/(x_b - x_a)$.

As shown in Fig. 6(b), some of the lines are blocked when there are stains. At this time, according to the positioning in array P[j], the contaminated and its symmetrical lines can be removed. In Fig. 6(b), the contaminated lines are x_2, x_3, and x_4, respectively. When calculating x_a, the reserved line group is {P[1], P[7]}; when calculating x_b, the reserved line group is {P[5]}. x_a and x_b are calculated by Eqs. (7) and (8), respectively:

$$x_a' = \frac{P[1] + P[7]}{2}, \tag{7}$$

$$x_b' = P[5]. \tag{8}$$

Similarly, the subdivision value is calculated according to $B' = 2^m \cdot (x_b - x_0)/(x_b - x_a)$. Only when the number of contaminated lines in the IDA is no more than three can the subdivision operation work normally. Therefore, the algorithm can remove the interference when the number of lines covered by the stains is less than half of the coding-bits.

2. Coding Value Acquisition

Because the line covered by the stain affects the accurate recognition of the coded value in the IDA, we recorded the change of the subdivision value B in real time to judge whether the decoding value A should be "carried," as shown in Fig. 7.

The subdivision value B of the previous time and the subdivision value B' of the next time are recorded; then the decoding value is judged by comparing B and B'. As shown in Fig. 7(a), when $B > 2^m \cdot 3/4$ and $B' < 2^m/4$, the decoding value should be "carried"; at this time, 1 is added to the current decoding value. As shown in Fig. 7(b), when $B < 2^m/4$ and

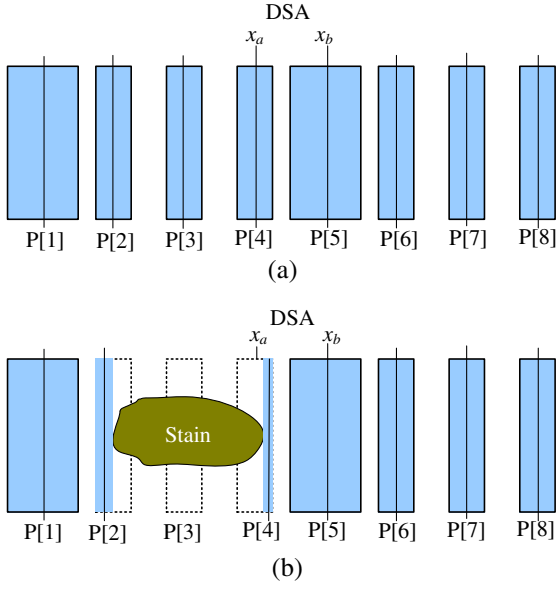

Fig. 6. Subdivision principle.

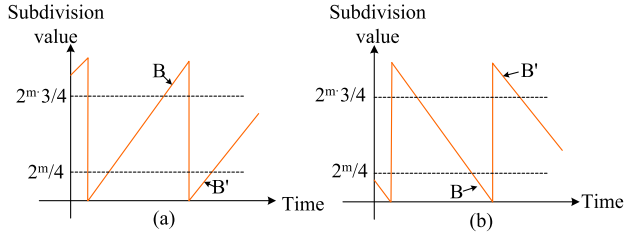

Fig. 7. Decoding value acquisition.

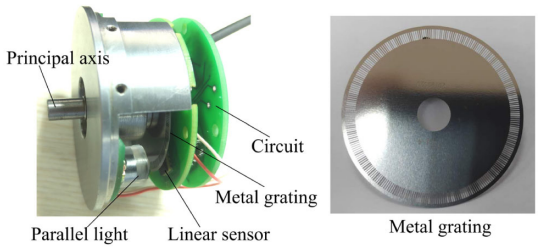

Fig. 8. Experimental device.

$B' > 2^m \cdot 3/4$, the decoding value should be "debited" and the current decoding value is reduced by 1. When the stains in the field of vision disappear, the coding of the lines continues to be used for decoding.

4. EXPERIMENT

A parallel light and metal grating were used to prototype the experimental device as shown in Fig. 8.

The experimental setup includes a parallel light source, metal grating, principal axis, linear image sensor, and processing circuit. The pixel size of the linear image sensor is 7.94 μm, and the resolution is 1×512 pixels; the wavelength of the parallel light source is 850 nm. The material of the metal grating is stainless steel, and there are $2^8 = 256$ coding lines in the circumference of the grating. In the subdivision operation, we made $2^m = 2^{13}$. The experimental device can realize 21-bit $(8 + 13)$ angle measurement.

Although the metal grating eliminates the interference from dust to a certain extent, the stains attached to the grating still block the coding lines. The anti-stain algorithm is needed to remove them.

A. Simulation

The image sensor collects pixel data during the measurement process as shown in Fig. 9. The position of the image center point is $x_0 = 256$, and the centroid array of eight lines on both sides of the center point is $\{P[1], P[2], P[3], P[4], P[5], P[6], P[7], P[8]\} = \{73.05, 125.77, 178.21, 231.28, 284.19, 337.20, 389.59, 442.60\}$. Per Eqs. (3) and (4), $x_a = 231.36$ and $x_b = 284.15$. The angle subdivision value B is $2^m \cdot (x_b - x_0)/(x_b - x_a) = 0.5332 \times 2^m$.

Suppose that there are stains covering the three lines P[2]−P[4] in Fig. 9. At this time, x_a and x_b calculated by the anti-stain algorithm are, respectively, $x_a = (P[1] + P[7])/2 = 231.32$ and $x_b = P[5] = 284.19$. The angle subdivision value is $B = 2^m \cdot (x_b - x_0)/(x_b - x_a) = 0.5332 \times 2^m$. There is little divergence from the subdivision value before the stain emerges, so the stain can be removed.

B. Numerical Output Experiment

We occluded a few lines on the calibration grating with tape to test the stain resistance [Fig. 10(a)]. We rotated the axis slowly to collect image and measurement output data for testing.

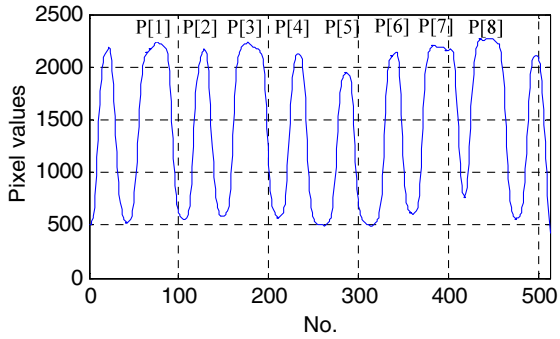

Fig. 9. Collected images.

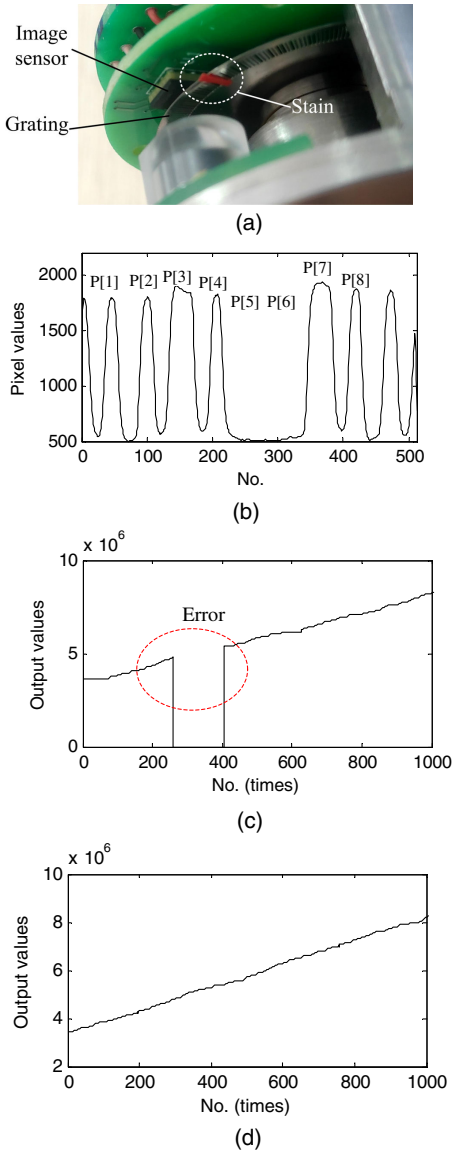

Fig. 10. Stain resistance tests.

The collected image of a stain in the IDA is shown in Fig. 10(b), where P[5] and P[6] are affected. Figure 10(c) shows the output data of angular displacement measurement

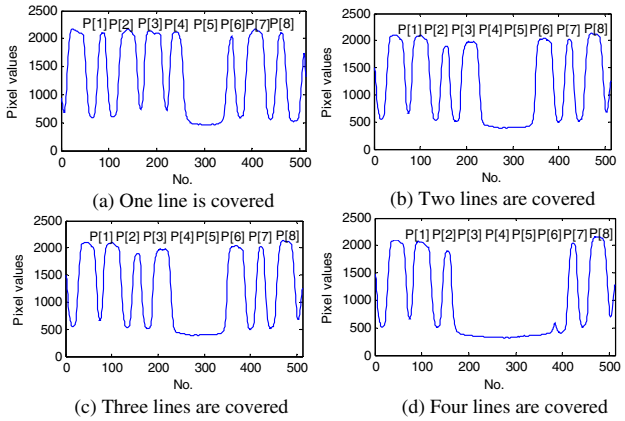

Fig. 11. Collected images of stain.

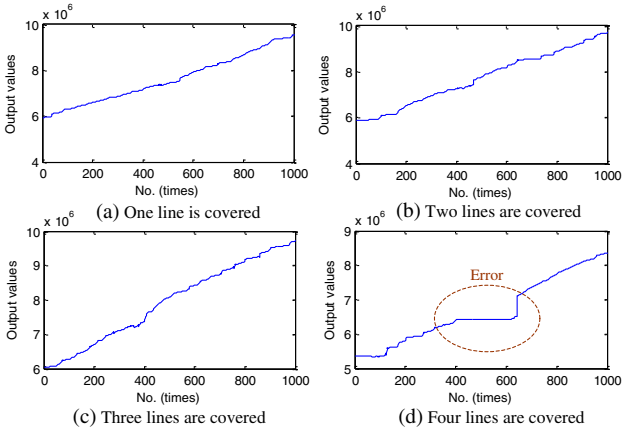

Fig. 12. Stain area tests.

without the anti-stain algorithm, where there is an output error in Fig. 10(c). Figure 10(d) shows the output data after the anti-stain algorithm, where the stain has no such effect. In short, the proposed algorithm is effective.

C. Stain Resistance Test

We next covered one, two, three, and four lines, respectively, and tested them for stain resistance. The collected images are shown in Figs. 11(a)–11(d).

Figures 12(a)–12(d) show the results of the four tests. The anti-stain algorithm produced a normal output when lines 1, 2, or 3 were blocked [Figs. 12(a)–12(c)]; when line 4 was blocked, the output angle data was stagnant and the anti-stain algorithm did not guarantee the measurement output [Fig. 12(d)]. In effect, the proposed algorithm can prevent stain-related interference when the number of stains is less than four.

5. CONCLUSIONS

An anti-stain algorithm was developed in this study to enhance the performance of image angular displacement measurement technology based on multi-line fusion. Experimental results indicated that the proposed algorithm can eliminate the interference of stains when the number of lines covered by the stains is less than half of the coding-bits. This work may provide a technical foundation for future high-performance angular displacement measurement technologies.

Funding. National Natural Science Foundation of China (51605465); Science and Technology Development Programme of Jilin Province (20180520184JH).

Acknowledgment. We thank the photoelectric displacement sensor group of the Precision Instrument and Equipment R&D Center, Changchun Institute of Optics, Fine Mechanics and Physics, Chinese Academy of Sciences.

Disclosures. The authors declare no conflicts of interest.

REFERENCES

1. K. Hane, T. Endo, M. Ishimori, and M. Sasaki, "Integration of grating-image-type encoder using Si micromachining," Sens. Actuators A, Phys. **97**, 139–146 (2002).
2. F. Liu, W. Wang, L. Wang, and P. Feng, "Error analyses and calibration methods with accelerometers for optical angle encoders in rotational inertial navigation systems," Appl. Opt. **52**, 7724–7731 (2013).
3. D. B. Leviton and M. S. Garza, "Recent advances and applications for NASA's new, ultra-high sensitivity, absolute, optical pattern recognition encoders," Proc. SPIE **4091**, 375–384 (2003).
4. D. B. Leviton and B. J. Frey, Ultra-high resolution, absolute position sensors for cytostatic applications," Proc. SPIE **4850**, 776–787 (2003).
5. Y. Sugiyam, Y. Matsu, H. Toyod, M. Takabe, S. Mizuno, Y. Matsui, H. Toyoda, and N. Mukozaka, "A 3.2 kHz 14-bit optical absolute rotary encoder with a CMOS profile sensor," IEEE Sens. J. **8**, 1430–1436 (2008).
6. J. Xu, W. Ye, X. Ni, and X. Cao, "Virtual Moiré fringe for grating measurement system based on CMOS microscopic imaging," Proc. SPIE **7853**, 785325 (2010).
7. J. S. Baji, D. Z. Stupara, B. M. Dakib, M. B. Živanov, and L. F. Nagy, "An absolute rotary position sensor based on cylindrical coordinate color space transformation," Sens. Actuators A, Phys. **213**, 27–34 (2014).
8. J. A. Kim, J. W. Kim, C. S. Kang, J. Jin, and T. B. Eom, "Absolute angle measurement using a phase-encoded binary graduated disk," Measurement **80**, 288–293 (2016).
9. P. Yuan, D. Huang, Z. Lei, and C. Xu, "An anti-spot, high-precision subdivision algorithm for linear CCD based single-track absolute encoder," Measurement **137**, 143–154 (2019).
10. Z. Zhang, F. Ni, Y. Dong, M. Jin, and H. Liu, "A novel absolute angular position sensor based on electromagnetism," Sens. Actuators A, Phys. **194**, 196–203 (2013).
11. H. Yu, Q. Wan, X. R. Lu, C. Zhao, and Y. Du, "A robust sub-pixel subdivision algorithm for image-type angular displacement measurement," Opt. Laser. Eng. **100**, 234–238 (2018).
12. H. Yu, Q. Wan, Y. Sun, X. Lu, and C. Zhao, "High-precision absolute angular displacement measurement via dual imaging detectors," IEEE Sens. J. **19**, 7308–7312 (2019).
13. H. Yu, X. Jia, Q. Wan, C. Zhao, and Y. Sun, "High-resolution angular measurement arithmetic based on pixel interpolations," Measurement **149**, 106948 (2020).
14. H. Yu, Q. Wan, X. Lu, Y. Du, and S. Yang, "Small-size, high-resolution angular displacement measurement technology based on an imaging detector," Appl. Opt. **56**, 755–760 (2017).